

UNIT-V

BATTERY CHARGING AND CONTROL

Battery charging: Basic requirements, charger architecture, charger functions, wireless charging, power factor correction.

Control: Introduction, modelling of electromechanical system, feedback controller design approach, PI controllers designing, torque-loop, speed control loop compensation, acceleration of battery electric vehicle

CHARGER FUNCTION:

An EV charger is a piece of equipment that supplies power for electric vehicles. Its main function is to **recharge** the battery of an EV to keep the vehicle in motion.

Most electric vehicles' batteries can only be charged with direct current (DC) power, yet some EV have a charger that converts alternating current (AC) electricity into DC and then sends this power to the vehicle's charging port.

5.1 CHARGER CLASSIFICATION:

A PHEV is a hybrid vehicle with a storage system that can be recharged by connecting a plug to an external electric power source through an AC or DC charging system. The AC charging system is commonly an on-board charger mounted inside the vehicle and is connected to the grid. The DC charging system is commonly an off-board charger mounted at fixed locations, supplying required regulated DC power directly to the batteries inside the vehicle.

5.1.1 AC Charging Systems

The charging AC outlet inevitably needs an on-board AC-DC charger with a power factor correction (PFC). Table 13.1 illustrates charge method electrical ratings according to SAE(Society of Automotive Engineers) EV AC charging power levels.

These chargers are classified by the level of power they can provide to the battery pack:

- **Level 1:** Common household circuit, rated up to 120 V AC and up to 16 A. These chargers use the standard three-prong household connection, and they are usually considered portable equipment.
- **Level 2:** Permanently wired electric vehicle supply equipment (EVSE) used especially for electric vehicle charging; rated up to 240 V AC, up to 60 A, and up to 14.4 kW.

TABLE 13.1
Charge Method Electrical Ratings—SAE EV AC Charging Power Levels

Charge Method	Nominal Supply Voltage	Maximum Current	Branch Circuit Breaker Rating	Output Power Level
AC level 1	120 V AC, 1-phase	12 A	15 A	1080 W
	120 V AC, 1-phase	16 A	20 A	1440 W
AC level 2	208–240 V AC, 1-phase	16 A	20 A	3300 W
	208–240 V AC, 1-phase	32 A	40 A	6600 W
	208–240 V AC, 1-phase	≤80 A	Per NEC 635	≤14.4 kW

- **Level 3:** Permanently wired EVSE used especially for electric vehicle charging; rated greater than 14.4 kW. Fast chargers are rated as level 3, but not all level 3 chargers are fast chargers. This designation depends on

the size of the battery pack to be charged and how much time is required to charge the battery pack. A charger can be considered a fast charger if it can charge an average electric vehicle battery pack in 30 min or less.

In summary

- AC chargers are commonly on-board the vehicle
- AC is supplied to the vehicle
- Charger supplies DC to the battery
- Must be automotive-grade components
- Considerations for reliability, thermal cycling, vibration, lifetime/warranty, and so on
- High cost to produce and low profit margins for suppliers
- AC levels 1 and 2 are the dominant technologies in production today

5.1.2 DC Charging Systems

The DC charging systems are mounted at fixed locations, like the garage or dedicated charging stations. Built with dedicated wiring, these chargers can handle much more power and can charge the batteries more quickly. However, as the output of these chargers is DC, each battery system requires the output to be changed for that car. Modern charging stations have a system for identifying the voltage of the battery pack and adjusting accordingly. Table 13.2 illustrates charge method electrical ratings according to SAE EV DC charging power levels.

These chargers are classified by the level of power they can provide to the battery pack:

- **Level 1:** Permanently wired EVSE includes the charger; rated 200–450 V DC, up to 80 A, and up to 36kW

TABLE 13.2
Charge Method Electrical Ratings—SAE EV DC Charging Power Levels

Charge Method	Supplied DC Voltage Range	Maximum Current	Power Level
DC level 1	200–450 V DC	≤80 A DC	≤36 kW
DC level 2	200–450 V DC	≤200 A DC	≤90 kW
DC level 3	200–600 V DC	≤400 A DC	≤240 kW

- **Level 2:** Permanently wired EVSE includes the charger; rated 200–450 V DC, up to 200 A, and up to 90 kW
- **Level 3:** Permanently wired EVSE includes the charger; rated 200–600 V DC, up to 400 A, and up to 240 kW

In summary

- DC chargers are off-board (not in the vehicle)
- AC supplied to a charging box
- Charger supplies DC to the vehicle
- Consumer-grade components
- Considerations for reliability, thermal cycling, vibration, and so on not as demanding
- Lower cost to produce and potentially increased profit margins
- DC level 3 Tesla superchargers limited availability

- EVSE includes an off-board charger

5.3 CHARGER REQUIREMENTS

Several considerations and regulatory standards must be met. The charger must comply with the following standards for safety:

- UL 2202: EV Charging System Equipment
- IEC(International electrotechnical commission) 60950: Safety of Information Technology Equipment
- IEC 61851-21: Electric Vehicle Conductive Charging System—Part 21: Electric Vehicle Requirements for Conductive Connection to an AC–DC Supply
- IEC 61000: Electromagnetic compatibility (EMC)
- ECE(Economic commission for Europe) R100: Protection against Electric Shock
- ISO 6469-3: Electric Road Vehicles—Safety Specifications—Part 3: Protection of Persons against Electric Hazards
- ISO(International organisation for standardization) 26262: Road Vehicles—Functional Safety
- SAE J2929: Electric and Hybrid Vehicle Propulsion Battery System Safety Standard
- FCC Part 15 Class B: The Federal Code of Regulation (CFR) FCC Part 15 for EMC Emission Measurement Services for Information Technology Equipment

In addition, it may be affected by high temperatures, vibration, dust, and other parameters, which comprise the operating environment. Therefore, the charger must meet the following operating environment:

- Engine compartment capable
- IP6K9K, IP6K7 protection class
- -40°C to 105°C ambient air temperature
- -40°C to 70°C liquid coolant temperature

The input and output requirements for a level 2, 3.3 kW charger are also given below.

Input:

- Input voltage range: 85–265 VAC
- Input frequency range: 45–70 Hz
- Input current: 16 A RMS max
- Power factor: ≥ 0.98

Output:

- Output voltage range: 170–440 V DC
- Output power: 3.3 kW max
- Output current: 12 A DC max
- High efficiency: $>94\%$

5.4 TOPOLOGY SELECTION FOR LEVEL 1 AND 2 AC CHARGERS. (Charger Architecture)

The front-end AC–DC converter is a key component of the charger system. A variety of circuit topologies and control methods have been developed for the PFC application. The single phase active PFC techniques can be divided into two categories: the single-stage approach and the two-stage approach. The single-stage approach is suitable for low-power applications. In addition, owing to large low-frequency ripple in the output current, only lead acid batteries are chargeable.

Furthermore, galvanic isolation is required in on-board battery chargers in order to meet the double fault protection for the safety of the users of PHEV. Therefore, the two-stage approach is the proper candidate for PHEV battery chargers, where the power rating is relatively high, and lithium-ion batteries are used as the main energy storage system. The front-end PFC section is then followed by a DC–DC section to complete the charger system.

Figure 13.1 illustrates a simplified block diagram of a universal input two-stage battery charger used for PHEVs and EVs. The PFC stage rectifies the input AC voltage and transfers it into a regulated intermediate DC link bus. At the same time, PFC function is achieved. The following DC–DC stage then converts the DC bus voltage into a regulated output DC voltage for charging batteries, which is required to meet the regulation and transient requirements.

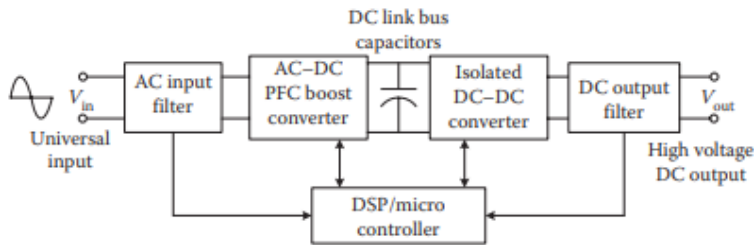


FIGURE 13.1 Simplified system block diagram of a universal on-board two-stage battery charger.

5.4.1 Front-end AC–DC Converter topologies (Power Factor Correction):

As a key component of a charger system, the front-end AC–DC converter must achieve high efficiency and high power density. Additionally, to meet the efficiency and power factor requirements and regulatory standards for the AC supply mains, PFC is essential. As the adoption rate of these vehicles increases, the stress on the utility grid is projected to increase significantly at times of peak demand. Therefore, efficient and high power factor charging is critical in order to minimize the utility load stress, and reduce the charging time. In addition, a high power factor is needed to limit the input current harmonics drawn by these chargers and to meet regulatory standards, such as IEC 1000-3-2.

According to the requirements of input current harmonics and output voltage regulation, a frontend converter is normally implemented by a PFC stage. Conventionally, most of the power conversion equipment employs either a diode rectifier or a thyristor rectifier with a bulk capacitor to convert AC voltage to DC voltage before processing it. Such rectifiers produce input current with rich harmonic content, which pollute the power system and the utility lines. Power quality is becoming a major concern for many electrical users.

The simplest form of PFC is passive (passive PFC). A passive PFC uses a filter at the AC input to correct poor power factor. The passive PFC circuitry uses only passive components—an inductor and some capacitors. Although pleasantly simple and robust, a passive PFC rarely achieves low total harmonic distortion (THD). Furthermore, because the circuit operates at the low line power frequency of 50 or 60 Hz, the passive elements are normally bulky and heavy. Figure 13.2 shows input voltage and current for a passive PFC and the harmonic spectrum of input current.

The input power factor (PF) is defined as the ratio of the real power over apparent power as

$$\text{Power factor (PF)} = \frac{\text{Real power (W)}}{\text{Apparent power (VA)}}$$

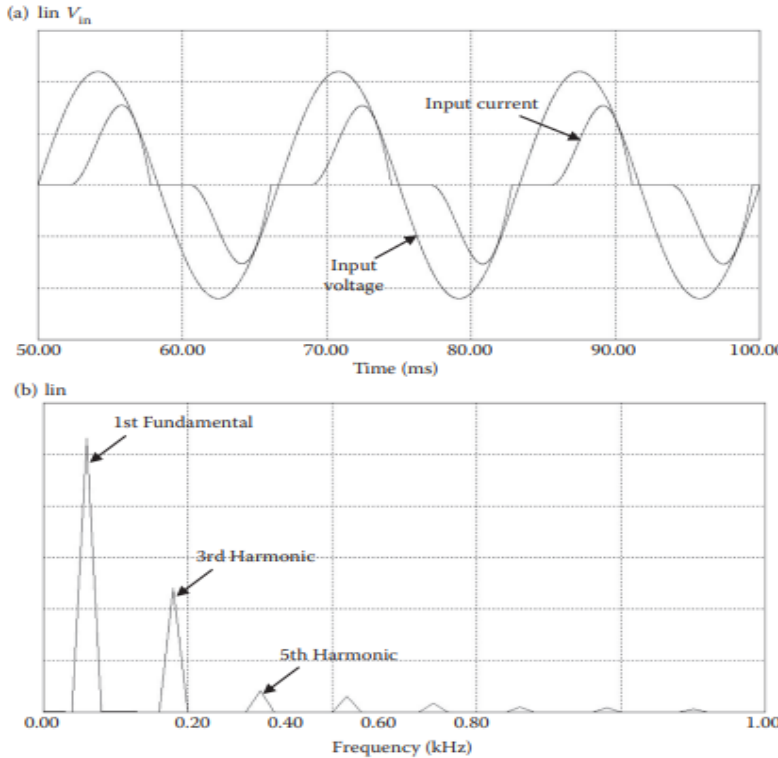


FIGURE 13.2 Passive power factor correction AC main voltage and current waveforms. (a) Input voltage and input current. (b) Harmonic spectrum of input current.

Assuming an ideal sinusoidal input voltage source, the power factor can be expressed as the product of two factors, the distortion factor and the displacement factor, given as

$$PF = K_d K_\theta$$

The distortion factor, K_d , is the ratio of the fundamental root mean square (RMS) current to the total RMS current.

a. Input voltage and input current

b. Harmonic spectrum of input current

The displacement factor, K_θ , is the cosine of the displacement angle between the fundamental input current and the input voltage fundamental RMS current.

$$K_d = \frac{I_{1\text{rms}}}{I_{\text{rms}}}$$

$$K_\theta = \cos \theta_i$$

where $I_{1\text{rms}}$ is the fundamental component of the line current, I_{rms} is the total line current, and θ_i is the phase shift of the current fundamental relative to the sinusoidal line voltage. The distortion factor is close to unity, even for waveforms with noticeable distortion; therefore, it is not a very convenient measure of distortion for

practical use. The distortion factor is uniquely related to another figure of merit: the THD.

$$\text{THD} = \sqrt{\frac{I_{\text{rms}}^2 - I_{\text{i rms}}^2}{I_{\text{i rms}}^2}}$$

$$K_d = \sqrt{\frac{1}{1 + \text{THD}^2}}$$

K_d is regulated by IEC 1000-3-2 for lower power levels and by IEEE Std 519-1992 for higher power levels, where $K\theta$ is regulated by utility companies. Significant reduction of current harmonics in single-phase circuits can only be achieved by using rectifiers based on pulse width modulated (PWM) switching converters. These converters can be designed to emulate a resistive load and, therefore, produce very little distortion of the current. By using PWM or other modulation techniques, these converters draw a nearly sinusoidal current from the AC line in phase with the line voltage. As a result, the rectifier operates with very low current harmonic distortion and very high, practically unity power factor. This technique is commonly known as PFC. As a result of this research, the existing PFC technology based on the boost converter topology with average-current-mode control was significantly improved. The proposed improvements allowed an extended range of operating conditions and additional functionality. The following section illustrates several common PFC topologies suitable for PHEV charger applications.

5.4.1.1 Conventional Boost PFC Converter

The conventional boost topology is the most popular topology for PFC applications. It uses a dedicated diode bridge to rectify the AC input voltage to DC, which is then followed by the boost section, as shown in Figure 13.3.

In this topology, the output capacitor ripple current is very high and is the difference between diode current and the DC output current. Furthermore, as the power level increases, the diode bridge losses significantly degrade the efficiency, so dealing with the heat dissipation in a limited area becomes problematic. The inductor volume also becomes a problematic design issue at high power. Another challenge is the power rating limitation for current sense resistors at high power.

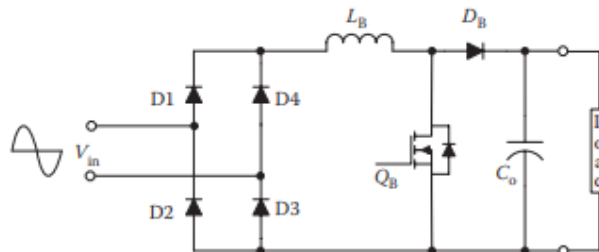


FIGURE 13.3 Conventional PFC boost converter.

5.4.1.2 Interleaved Boost PFC Converter

The interleaved boost converter, illustrated in Figure 13.4, consists of two boost converters in parallel operating at 180° out of phase.

The input current is the sum of the two input inductor currents. Because the inductors' ripple currents are out of phase, they tend to cancel each other and reduce the input ripple current caused by the boost switching action. The interleaved boost converter has the advantage of paralleled semiconductors. Furthermore, by switching 180° out of phase, it doubles the effective switching frequency and introduces smaller input current ripple, so the input EMI filter is relatively small [9,10]. With ripple cancellation at the output, it also reduces stress on output capacitors.

5.4.1.3 Bridgeless Boost PFC Converter

The bridgeless boost topology, illustrated in Figure 13.5, is the second topology considered for this application. The gates of the powertrain switches are tied together, so the gating signals are identical, as is illustrated in Figure 13.6. It avoids the need for the rectifier input bridge, yet maintains

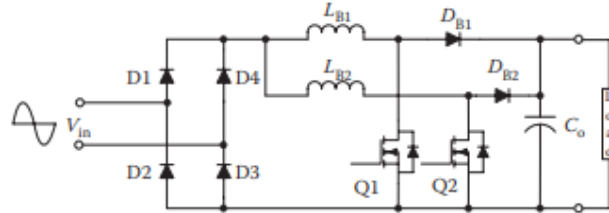


FIGURE 13.4 Interleaved PFC boost converter.

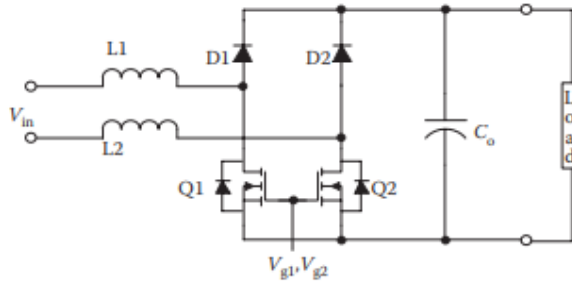


FIGURE 13.5 Bridgeless PFC boost topology.

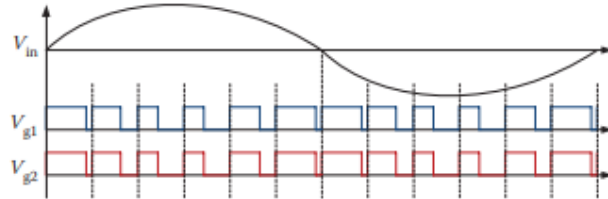


FIGURE 13.6 Gating scheme for the bridgeless PFC boost topology illustrating the identical gating signals for both MOSFETs.

the classic boost topology. It is an attractive solution for applications >1 kW, where power density and efficiency are important. The bridgeless boost converter, also known as dual-boost PFC converter, solves the problem of heat management in the input rectifier diode bridge, but it introduces increased electromagnetic interference (EMI). This is because the amplitude of the noise source applied to the stray capacitor from high-voltage DC bus and power ground is a lot higher in bridgeless PFC; as a result, the common mode (CM) noise generated by bridgeless PFC is much higher than conventional boost PFC topology. Another disadvantage of this topology is the floating input line with respect to the PFC stage ground, which makes it impossible to sense the input voltage without a low-frequency transformer or an optical coupler.

5.4.1.4 Dual-Boost PFC Converter

The dual-boost converter, illustrated in Figure 13.7, is an alternative adaptation of the bridgeless boost topology [18]. In this topology, the MOSFET gates are decoupled, enabling one of the switches to remain on and operate as a synchronous MOSFET for half-line cycle. Figure 13.8 illustrates the gating scheme for a dual-boost PFC topology. The dual-boost topology reduces gate loss, and at light loads, conduction loss can be reduced until the voltage drop across the MOSFET channel RDS(ON) becomes equal to the voltage drop across the MOSFET body diode, at which point any additional current conducts through the body diode. The light load efficiency improvement comes at the expense of the cost of an additional driver and increased controller complexity.

5.4.1.5 Semi-Bridgeless Boost PFC Converter

The semi-bridgeless configuration, shown in Figure 13.9, includes the conventional bridgeless topology with two additional slow diodes, Da and Db, that connect the input to the PFC ground [19]. The slow diodes were added to address EMI-related issues [15,16]. The current does not always return through these diodes, so their associated conduction losses are low. This occurs since the inductors exhibit low impedance at the line frequency, so a large portion of the current flows through the MOSFET intrinsic body diodes. The semi-bridgeless configuration also resolves the floating input line problem with respect to the PFC stage ground. The topology change enables input voltage sensing using a string of simple voltage dividers.

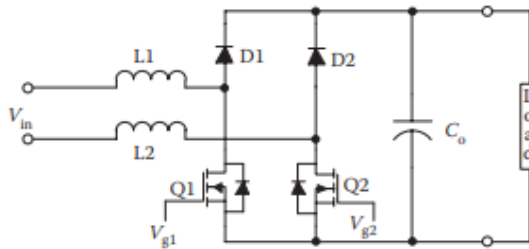


FIGURE 13.7 Dual-boost PFC topology.

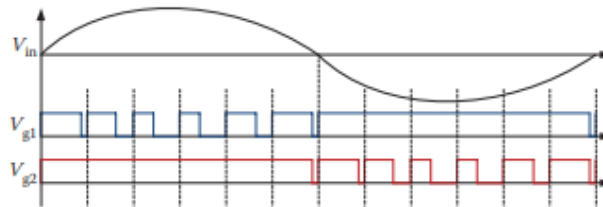


FIGURE 13.8 Gating scheme for the dual-boost PFC topology illustrating half-line cycle synchronous rectification.

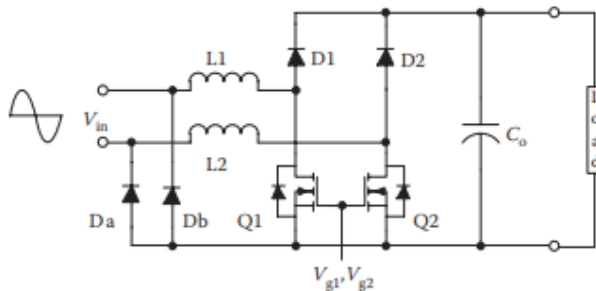


FIGURE 13.9 Semi-bridgeless PFC boost topology.

5.4.1.6 Bridgeless Interleaved Boost PFC Converter

The bridgeless interleaved topology, shown in Figure 13.10, was proposed as a solution to operate at power levels above 3.5 kW. In comparison to the interleaved boost PFC, it introduces two MOSFETs and also replaces four slow diodes with two fast diodes. The gating signals are 180° out of phase, similar to the interleaved boost. A detailed converter description and steady-state operation analysis are given in Reference 20. This converter topology shows a high input power factor, high efficiency over the entire load range, and low input current harmonics. Since the proposed topology shows high input power factor, high efficiency over the entire load range, and low input current harmonics, it is a potential option for single-phase PFC in high-power level 2 battery charging applications.

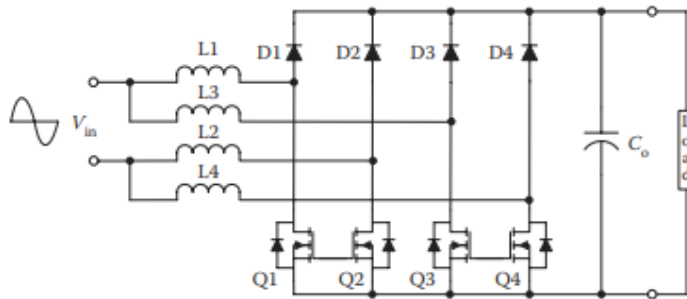


FIGURE 13.10 Bridgeless interleaved PFC boost converter. (From F. Musavi; W. Eberle; W.G. Dunford,

5.5 WIRELESS CHARGERS

5.5.1 Introduction

On-board chargers are burdened by the need for a cable-and-plug charger, galvanic isolation of the on-board electronics, the size and weight of the charger, and safety and issues with operating in rain and snow. Wireless power transfer (WPT) is an approach that provides a means to address these problems and offers the consumers a seamless and convenient alternative to charging conductively. In addition, it provides an inherent electrical isolation and reduces on-board charging cost, weight, and volume. A typical closed-loop inductive WPT charging system is illustrated in Figure 13.20. The basic principle of inductive WPT charging is that the two halves of the inductive coupling interface consist of the primary and secondary of a two-part transformer. The charger converts the low frequency AC utility power to high-frequency AC power in the power conversion stage. The secondary side wirelessly receives high-frequency AC from the charger, which is converted to DC by a rectifier, which then supplies the battery pack.

A two-part transformer behaves like mutual-inductively coupled or magnetically coupled inductors configured such that a change in current flow through one winding induces a voltage across the ends of the other winding through electromagnetic induction, as shown in Figure 13.21.

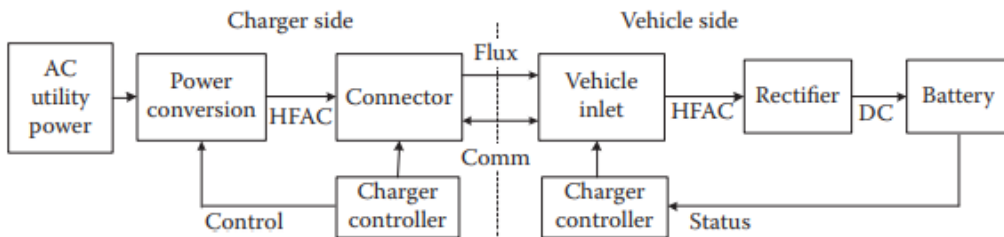


FIGURE 13.20 Typical closed-loop WPT charging systems.

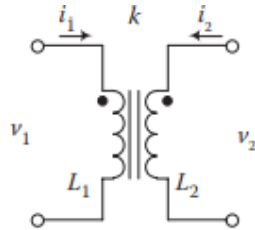


FIGURE 13.21 Coupled inductor circuit symbol.

The inductive coupling between two conductors is given by Equations

$$v_1 = L_1 \frac{di_1}{dt} + M \frac{di_2}{dt}$$

$$v_2 = L_2 \frac{di_2}{dt} + M \frac{di_1}{dt}$$

In above Equations, M denotes the mutual inductance, as given by the below Equation, where k is the coupling coefficient of the windings, or the quality of the magnetic circuit.

$$M = k \sqrt{L_1 L_2}$$

For a current I_1 in L_1 , the open circuit voltage induced in L_2 is given by

$$V_{OC} = \omega M I_1$$

With a short circuit on the right-hand side, the current is given by Equation

$$I_{SC} = \frac{V_{OC}}{\omega L_1} = I_1 \frac{M}{L_2}$$

When the system is tuned at the operating frequency with a capacitor, the available power is $V_{OC} I_{SC}$ multiplied by the circuit tuning resonant factor Q, and is given by,

$$P = \omega \frac{M^2}{L_2} I_1^2 Q = \omega L_1 I_1 I_1 \frac{M^2}{L_1 L_2} Q = V_1 I_1 k^2 Q$$

where Q is given by.

$$Q = \frac{\omega L}{R_L}$$

The power that an inductive WPT system can produce is therefore dependent on the input voltage–ampere product (VA) to the primary pad, the quality of the magnetic circuit (k), and the quality of the secondary electric circuit (Q).

5.5.2 Inductive Charging

In the 1990s, electric vehicles used inductive charging. An inductive charger uses mutual inductance to transfer electrical energy from the source to the vehicle. This works much the way a transformer works. In this system, an insulated paddle containing an electrically energized primary coil is brought close to a secondary coil within the vehicle. The magnetic field of the primary coil then induces a charge in the secondary coil.

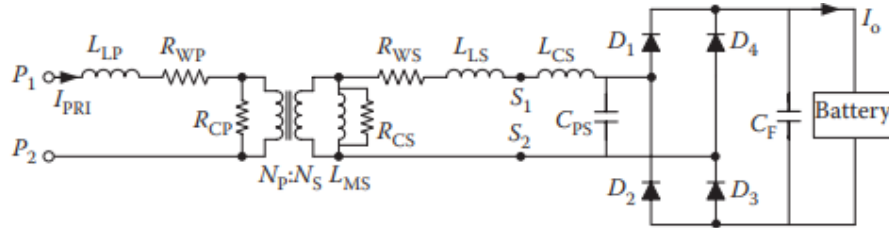


FIGURE 13.22 Inductive interface (paddle) equivalent circuit.

The charging paddle (the primary coil) of the Magne Charge inductively coupled charger was sealed in epoxy as was the secondary. The paddle inserted into the center of the secondary coil permitted charging of the EV1 without any contacts or connectors at either 6.6 or 50 kW. It should be noted that this system is connectorless, but not wireless. The equivalent circuit parameters at the charge coupling interface for an IPT charger are shown in Figure 13.22.

5.5.3 Resonant inductive Charging

Resonant inductive power transfer (RIPT) is the most popular current WPT technology. It was pioneered by Nikola Tesla and has recently become popular again, enabled by modern electronic components. This technique uses two or more tuned resonant tanks resonating at the same frequency.

A typical schematic of an RIPT system is illustrated in Figure 13.23. The receiver and transmitter contain resonant capacitors, C_p and C_s . The primary functions of the resonant circuits include

- Maximizing the transferred power
- Optimizing the transmission efficiency
- Controlling the transmitted power by frequency variation
- Creating a certain source characteristic (current or voltage source)
- Compensating variation of the magnetic coupling
- Compensating the magnetizing current in the transmitter coil to reduce generator losses
- Matching the transmitter coil impedance to the generator
- Suppressing higher harmonics from the generator

Efficient resonant magnetic power coupling can be achieved at distances up to approximately 40 cm. RIPT systems have several advantages over IPT, including increased range, reduced EMI, higher-frequency operation, resonant switching of the inverter and receiver rectification circuitry, and higher efficiency. However, the main advantage of this concept is that the operating frequency is in the kHz range, which can be supported by current state-of-the-art power electronics technologies.

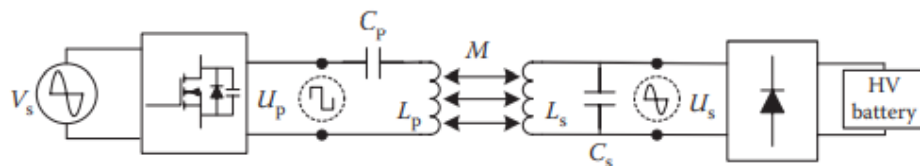


FIGURE 13.23 Simplified typical schematic of a resonant inductive charger.

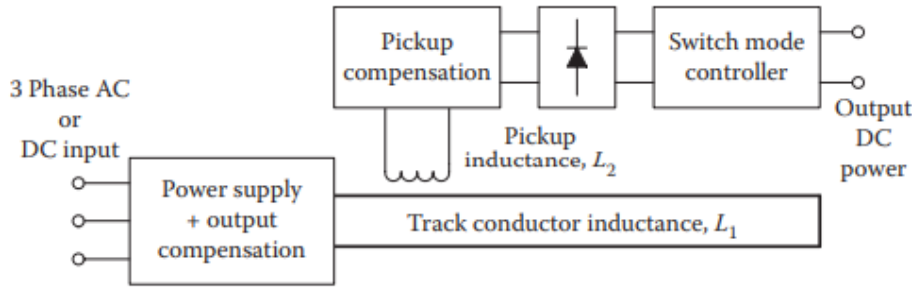


FIGURE 13.24 A typical on-line wireless power transfer system [49–58].

5.5.4 Roadway/on-line Charging

An on-line wireless power transfer system (OLPT) is illustrated in Figure 13.24. The concept is similar to RIPT; however, a lower resonant frequency is used and the technology has the potential for application at high power levels. Technologically, the primary coil is spread out over an area on the roadway and the power transfer happens at multiple locations within this area. Typically, the combination of the input side of the resonant converter along with the distributed primary windings is called the track and is on the road, and the secondary is called the pickup coil, which is in the vehicle. The system is supplied by a three-phase AC system, or high-voltage DC system.

Considering both the short range of EVs and the associated cost of infrastructure, the feasibility of these charging systems might be unfavourable. However, one benefit is that due to frequent and convenient charging, vehicles can be built with a minimal battery capacity (about 20% compared to that of the conventional battery-powered electric vehicles), which can consequently minimize the weight and the price of the vehicle.

DESIGNING FEEDBACK CONTROLLERS FOR MOTOR DRIVES

13-1 INTRODUCTION

Many applications, such as robotics and factory automation, require precise control of speed and position. In such applications, a feedback control, as illustrated by Fig. 13-1, is used. This feedback control system consists of a power-processing unit (PPU), a motor, and a mechanical load. The output variables such as torque and speed are sensed and are fed back, to be compared with the desired (reference) values. The error between the reference and the actual values are amplified to control the power-processing unit to minimize or eliminate this error. A properly designed feedback controller makes the system insensitive to disturbances and changes in the system parameters.

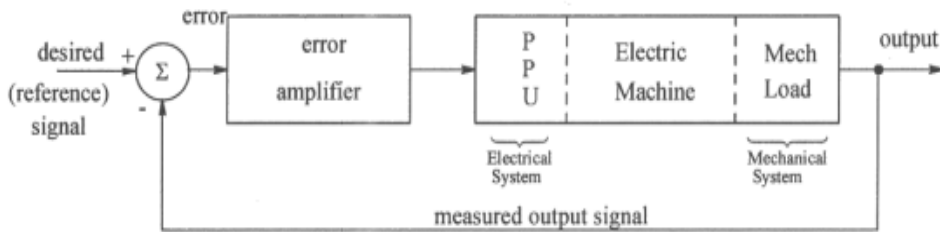


Fig 13-1 Feedback controlled drive.

The objective of this chapter is to discuss the design of motor-drive controllers. A dc-motor drive is used as an example, although the same design concepts can be applied in controlling brushless-dc motor drives and vector-controlled induction-motor drives. In the following discussion, it is assumed that the power-processing unit is of a switch-mode type and has a very fast response time. A permanent-magnet dc machine with a constant field flux ϕ_f is assumed.

13-2 CONTROL OBJECTIVES

The control system in Fig. 13-1 is shown simplified in Fig. 13-2, where $G_p(s)$ is the Laplace-domain transfer function of the plant consisting of the power-processing unit, the motor, and the mechanical load. $G_c(s)$ is the controller transfer function. In response to a desired (reference) input $X^*(s)$, the output of the system is $X(s)$, which (ideally) equals the reference input. The controller $G_c(s)$ is designed with the following objectives in mind:

- a zero steady state error.
- a good dynamic response (which implies both a fast transient response, for example to a step-change in the input, and a small settling time with very little overshoot).

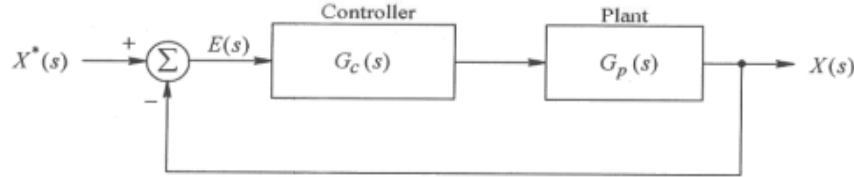


Fig 13-2 Simplified control system representation.

13-3 CASCADE CONTROL STRUCTURE

In the following discussion, a cascade control structure such as that shown in Fig. 13-4 is used. The cascade control structure is commonly used for motor drives because of its flexibility. It consists of distinct control loops; the innermost current (torque) loop is followed by the speed loop. If position needs to be controlled accurately, the outermost position loop is superimposed on the speed loop. Cascade control requires that the bandwidth (speed of response) increase towards the inner loop, with the torque loop being the fastest and the position loop being the slowest. The cascade control structure is widely used in industry.

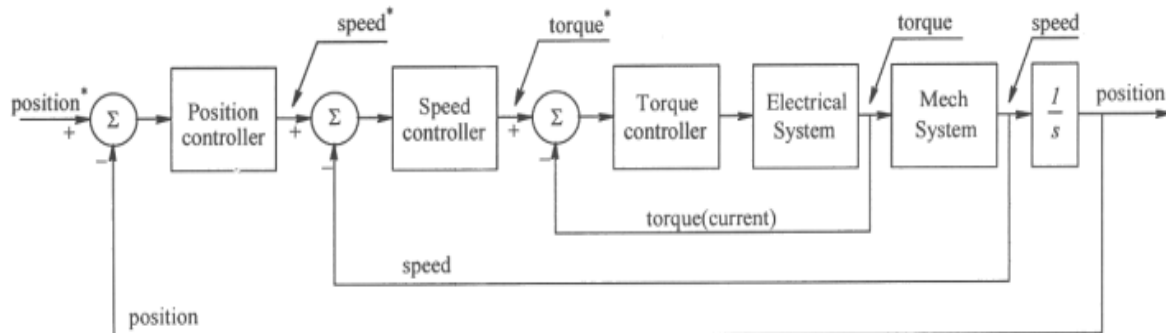


Figure 13-4 Cascade control of a motor drive.

13-5-2 Modeling of the DC Machine and the Mechanical Load

The dc motor and the mechanical load are modeled as shown by the equivalent circuit in Fig. 13-6a, in which the speed $\omega_m(t)$ and the back-emf $e_a(t)$ are assumed not to contain switching-frequency components. The electrical and the mechanical equations corresponding to Fig. 13-6a are

$$\bar{v}_a(t) = e_a(t) + R_a \bar{i}_a(t) + L_a \frac{d}{dt} \bar{i}_a(t), \quad e_a(t) = k_E \omega_m(t) \quad (13-7)$$

and

$$\frac{d}{dt} \omega_m(t) = \frac{\bar{T}_{em}(t) - T_L}{J_{eq}}, \quad \bar{T}_{em}(t) = k_T \bar{i}_a(t) \quad (13-8)$$

where the equivalent load inertia J_{eq} ($= J_M + J_L$) is the sum of the motor inertia and the load inertia, and the damping is neglected (it could be combined with the load torque T_L). In the simplified procedure presented here, the controller is designed to follow the changes in the torque, speed, and position reference values (and hence the load torque in Eq. 13-8 is assumed to be absent). Eqs. 13-7 and 13-8 can be expressed in the Laplace domain as

$$V_a(s) = E_a(s) + (R_a + sL_a)I_a(s) \quad (13-9)$$

or

$$I_a(s) = \frac{V_a(s) - E_a(s)}{R_a + sL_a}, \quad E_a(s) = k_E \omega_m(s) \quad (13-10)$$

We can define the Electrical Time Constant τ_e as

$$\tau_e = \frac{L_a}{R_a} \quad (13-11)$$

Therefore, Eq. 13-10 can be written in terms of τ_e as

$$I_a(s) = \frac{1/R_a}{1 + \frac{s}{1/\tau_e}} \{V_a(s) - E_a(s)\}, \quad E_a(s) = k_E \omega_m(s) \quad (13-12)$$

From Eq. 13-8, assuming the load torque to be absent in the design procedure,

$$\omega_m(s) = \frac{\bar{T}_{em}(s)}{s J_{eq}}, \quad \bar{T}_{em}(s) = k_T I_a(s) \quad (13-13)$$

Eqs. 13-10 and 13-13 can be combined and represented in block-diagram form, as shown in Fig. 13-6b.

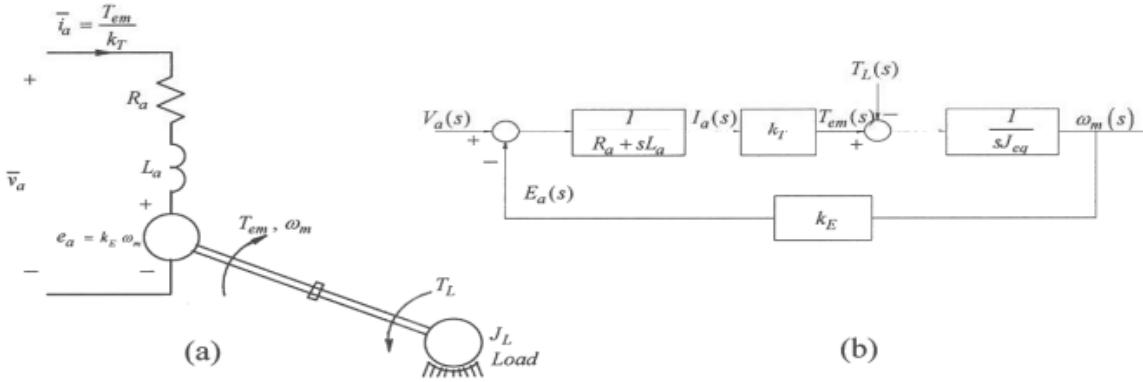


Fig 13-6 DC motor and mechanical load (a) equivalent circuit; (b) block diagram.

13-6 CONTROLLER DESIGN

The controller in the cascade control structure shown in Fig. 13-4 is designed with the objectives discussed in section 13-2 in mind. In the following section, a simplified design procedure is described.

13-6-1 PI Controllers

Motion control systems often utilize a proportional-integral (PI) controller, as shown in Fig. 13-7. The input to the controller is the error $E(s) = X^*(s) - X(s)$, which is the difference between the reference input and the measured output.

In Fig. 13-7, the proportional controller produces an output proportional to the error input:

$$V_{c,p}(s) = k_p E(s) \quad (13-14)$$

where k_p is the proportional-controller gain. In torque and speed loops, proportional controllers, if used alone, result in a steady-state error in response to step-change in the input reference. Therefore, they are used in combination with the integral controller described below.

In the integral controller shown in Fig. 13-7, the output is proportional to the integral of the error $E(s)$, expressed in the Laplace domain as

$$V_{c,i}(s) = \frac{k_i}{s} E(s) \quad (13-15)$$

where k_i is the integral-controller gain. Such a controller responds slowly because its action is proportional to the time integral of the error. The steady-state error goes to zero

for a step-change in input because the integrator action continues for as long as the error is not zero.

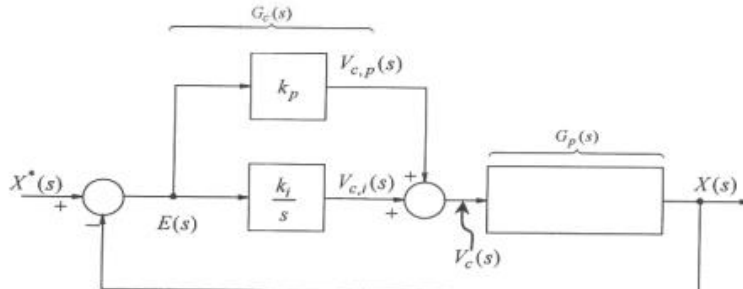


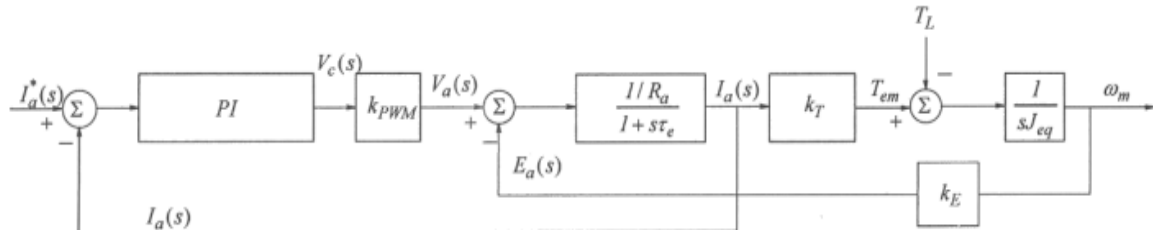
Figure 13-7 PI controller.

In motion-control systems, the P controllers in the position loop and the PI controllers in the speed and torque loop are often adequate. Therefore, we will not consider differential (D) controllers. As shown in Fig. 13-7, $V_c(s) = V_{c,p}(s) + V_{c,I}(s)$. Therefore, using Eqs. 13-14 and 13-15, the transfer function of a PI controller is

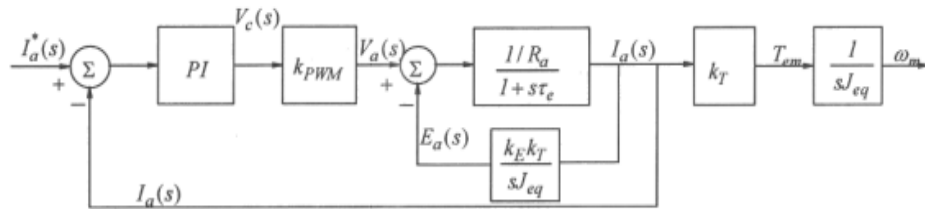
$$\frac{V_c(s)}{E(s)} = (k_p + \frac{k_I}{s}) = \frac{k_I}{s} [1 + \frac{s}{k_I/k_p}] \quad (13-16)$$

13-7-1 The Design of the Torque (Current) Control Loop

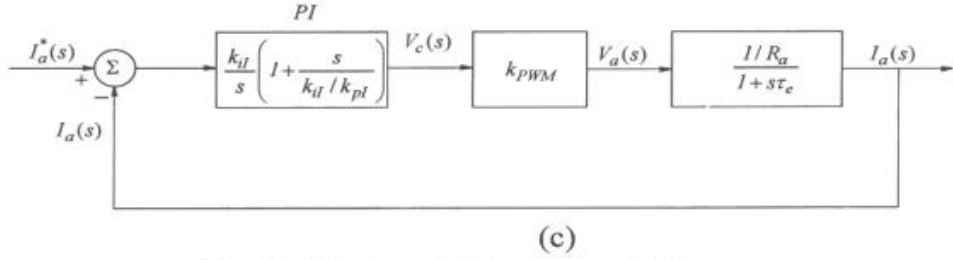
As mentioned earlier, we will begin with the innermost loop in Fig. 13-8a (utilizing the transfer function block diagram of Fig. 13-6b to represent the motor-load combination, Fig. 13-5c to represent the PPU, and Fig. 13-7 to represent the PI controller).



(a)



(b)



(c)

Fig. 13-8 Design of the torque control loop.

In permanent-magnet dc motors in which ϕ_f is constant, the current and the torque are proportional to each other, related by the torque constant k_T . Therefore, we will consider the current to be the control variable because it is more convenient to use. Notice that there is a feedback in the current loop from the output speed. This feedback dictates the induced back-emf. Neglecting T_L , and considering the current to be the output, $E_a(s)$ can be calculated in terms of $I_a(s)$ in Fig. 13-8a as $E_a(s) = \frac{k_T k_E}{s J_{eq}} I_a(s)$. Therefore, Fig. 13-8a can be redrawn as shown in Fig. 13-8b. Notice that the feedback term depends

inversely on the inertia J_{eq} . Assuming that the inertia is sufficiently large to justify neglecting the feedback effect, we can simplify the block diagram, as shown in Fig. 13-8c.

The current-controller in Fig. 13-8c is a proportional-integral (PI) error amplifier with the proportional gain k_{pl} and the integral gain k_H . Its transfer function is given by Eq. 13-16. The subscript “I” refers to the current loop. The open-loop transfer function $G_{I,OL}(s)$ of the simplified current loop in Fig. 13-8c is

$$G_{I,OL}(s) = \underbrace{\frac{k_H}{s} \left[1 + \frac{s}{k_H/k_{pl}} \right]}_{\text{PI-controller}} \underbrace{\frac{k_{PWM}}{PPU}}_{\text{motor}} \underbrace{\frac{1/R_a}{1 + \frac{s}{1/\tau_e}}}_{\text{motor}} \quad (13-17)$$

13-7-2 The Design of the Speed Loop

We will select the bandwidth of the speed loop to be one order of magnitude smaller than that of the current (torque) loop. Therefore, the closed-current loop can be assumed ideal for design purposes and represented by unity, as shown in Fig. 13-10. The speed controller is of the proportional-integral (PI) type. The resulting open-loop transfer function $G_{\Omega,OL}(s)$ of the speed loop in the block diagram of Fig. 13-10 is as follows, where the subscript “ Ω ” refers to the speed loop:

$$G_{\Omega,OL}(s) = \underbrace{\frac{k_{i\Omega}}{s} [1 + s / (k_{i\Omega} / k_{p\Omega})]}_{PI \text{ controller}} \underbrace{\frac{1}{s^2}}_{current \text{ loop}} \underbrace{\frac{k_T}{sJ_{eq}}}_{torque+inertia} \quad (13-21)$$

Eq. 13-21 can be rearranged as

$$G_{\Omega,OL}(s) = \left(\frac{k_{i\Omega} k_T}{J_{eq}} \right) \frac{1 + s / (k_{i\Omega} / k_{p\Omega})}{s^2} \quad (13-22)$$

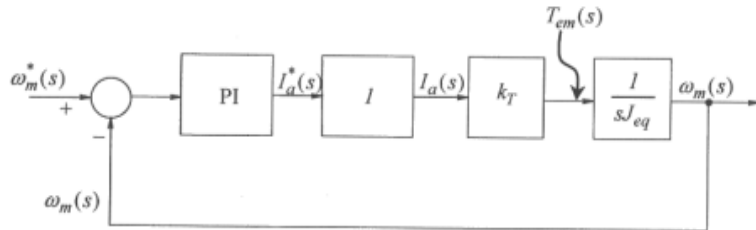


Fig 13-10 Block diagram of the speed loop.

13-7-3 The Design of the Position Control Loop

We will select the bandwidth of the position loop to be one order of magnitude smaller than that of the speed loop. Therefore, the speed loop can be idealized and represented by unity, as shown in Fig. 13-12. For the position controller, it is adequate to have only a proportional gain $k_{p\theta}$ because of the presence of a true integrator ($1/s$) in Fig. 13-12 in the open-loop transfer function. This integrator will reduce the steady state error to zero for a step-change in the reference position. With this choice of the controller, and with the closed-loop response of the speed loop assumed to be ideal, the open-loop transfer function $G_{\theta,OL}(s)$ is

$$G_{\theta,OL}(s) = \frac{k_\theta}{s} \quad (13-25)$$

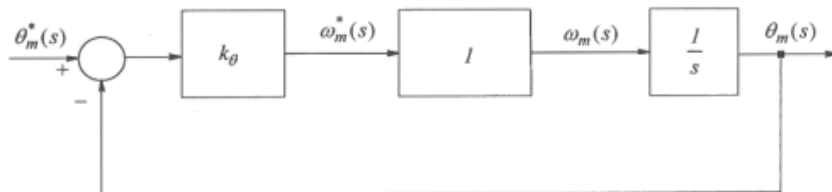


Fig 13-12 Block diagram of position loop.

Acceleration Force:

If the velocity of the vehicle is changing, then clearly a force will need to be applied in addition to the forces. This force will provide the linear acceleration of the vehicle, and is given by the well-known equation derived from Newton's third law,

$$F_{la} = ma \quad (8.4)$$

However, for a more accurate picture of the force needed to accelerate the vehicle we should also consider the force needed to make the rotating parts turn faster. In other words, we need to consider rotational acceleration as well as linear acceleration. The main issue here is the electric motor – not necessarily because of its particularly high moment of inertia, but because of the higher angular speeds.

Referring to Figure 8.2, clearly the axle torque equals $F_{te}r$, where r is the radius of the tyre and F_{te} is the tractive effort delivered by the powertrain. If G is the gear ratio of the system connecting the motor to the axle and T is the motor torque, then we can say that

$$T = \frac{F_{te}r}{G} \quad \text{and} \quad F_{te} = \frac{G}{r}T \quad (8.5)$$

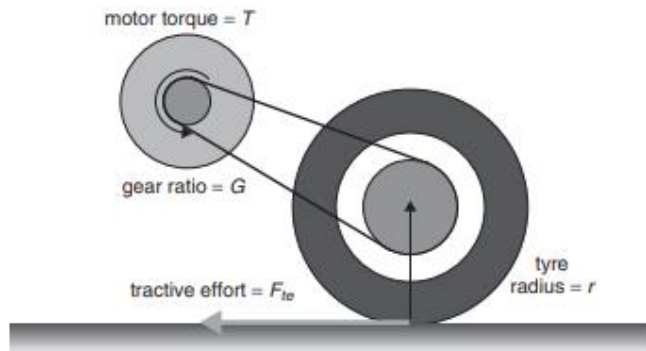


Figure 8.2 A simple arrangement for connecting a motor to a drive wheel

We will use this equation again when we develop final equations for vehicle performance. We should also note axle angular speed equals v/r radians per second, so motor angular speed is

$$\omega = G \frac{v}{r} \text{ rad s}^{-1} \quad (8.6)$$

and, similarly, motor angular acceleration is

$$\dot{\omega} = G \frac{a}{r} \text{ rad s}^{-2}$$

The torque required for this angular acceleration is

$$T = I \times G \frac{a}{r}$$

where I is the moment of inertia of the rotor of the motor. The force at the wheels needed to provide the angular acceleration (F_{wa}) is found by combining this equation with Equation (8.5), giving

$$F_{wa} = G \frac{r}{r} \times I \times G \frac{a}{r} \quad \text{or} \quad F_{wa} = I \frac{G^2}{r^2} a \quad (8.7)$$

Modelling of Vehicle Acceleration:

The maximum torque of an electric motor is a fairly simple function of angular speed. In most cases, at low speeds, the maximum torque is a constant, until the motor speed reaches a critical value ω_c after which the torque falls. In the case of a 'brushed' shunt or permanent magnet (PM) DC motor the torque falls linearly with increasing speed. In the case of most other types of motor, the torque falls in such a way that the power remains constant. The angular velocity of the motor depends on the gear ratio G and the radius of the drive wheel r as in Equation (8.6) derived above. So, we can say that

$$\text{For } \omega < \omega_c, \text{ or } v < \frac{r}{G} \omega_c, \text{ then } T = T_{\max}$$

Once this constant torque phase is passed, that is $\omega \geq \omega_c$, or $v \geq (r/G) \omega_c$, then either the power is constant, as in most brushless type motors, and we have

$$T = \frac{T_{\max} \omega_c}{\omega} = \frac{r T_{\max} \omega_c}{G v} \quad (8.10)$$

or the torque falls according to the linear equation we met in Section 7.1.2:

$$T = T_0 - k\omega$$

which, when Equation (8.6) is substituted for angular speed, gives

$$T = T_0 - \frac{kG}{r} v \quad (8.11)$$

Now that we have the equations we need, we can combine them in order to find the acceleration of a vehicle. Many of these equations may look quite complex, but nearly all the terms are constants, which can be found or estimated from vehicle or component data.

For a vehicle on level ground, with air density 1.25 kg m^{-3} , Equation (8.9) becomes

$$F_{te} = \mu_{rr} mg + 0.625 A C_d v^2 + ma + I \frac{G^2}{\eta_g r^2} a$$

Substituting Equation (8.5) for F_{te} , and noting that $a = dv/dt$, we have

$$\frac{G}{r} T = \mu_{rr} mg + 0.625 A C_d v^2 + \left(m + I \frac{G^2}{\eta_g r^2} \right) \frac{dv}{dt} \quad (8.12)$$

Modelling the Acceleration of a Small Car

For our example we will use a vehicle that had an important impact on the recent development of electric cars. The GM EV1 was arguably the first modern electric car from one of the really large motor companies. It incorporated technologies that were quite novel when it was introduced. But as far as simulating its performance, the main features are:

- an ultra-low drag coefficient C_d of 0.19;
- a very low coefficient of rolling resistance, μ_{rr} , of 0.0048;
- the use of variable frequency induction motors, operating at very high speed – nearly 12 000 rpm at maximum speed.

Further data is taken from company information¹ about the vehicle:

- Vehicle mass = 1400 kg.² Then add a driver and a passenger each weighing 70 kg, giving $m = 1540$ kg.
- The motor's moment of inertia is not known. However, compared with the mass of such a heavy vehicle this will be very low. The wheels are also very light. We will approximate this term by increasing the mass very modestly to 1560 kg in the final term of Equation (8.12).
- The gear ratio is 11:1, thus $G = 11$. The tyre radius is 0.30 m.
- For the motor, $T_{\max} = 140$ N m and $\omega_c = 733$ rad s⁻¹ (Note that this means $T = T_{\max}$ till $v = 19.8$ m s⁻¹ (71.3 kph)).
- Above 19.8 m s⁻¹ the motor operates at a constant 102 kW, as this is a WOT test. So

$$T = \frac{102000}{37 \times v} = \frac{2756}{v}$$

- The frontal area $A = 1.8$ m².
- The efficiency of the single-speed drive coupling between motor and axle is estimated as 95%, so $\eta_o = 0.95$. The values of the torque T will be reduced by a factor of 0.95.